A Virtual Reference Point Kinematic Guidance Law for 3-D Path-Following of Autonomous Underwater Vehicles

Loïck Degorre, Thor I Fossen, Emmanuel Delaleau, Olivier Chocron

IEEE Access
Multidisciplinary | Rapid Review | Open Access Journal

IEEE Systems, Man and Cybernetics Society Section

Received 14 July 2024, accepted 2 August 2024, date of publication 8 August 2024, date of current version 19 August 2024.

Digital Object Identifier 10.1109/ACCESS.2024.3440659

APPLIED RESEARCH

A Virtual Reference Point Kinematic Guidance Law for 3-D Path-Following of Autonomous Underwater Vehicles

LOÏCK DEGORRE[1], THOR I. FOSSEN[2], (Fellow, IEEE), EMMANUEL DELALEAU[3], AND OLIVIER CHOCRON[3]

[1]LABSTICC UMR 6285, ENSTA Bretagne, 29200 Brest, France
[2]Department of Engineering Cybernetics, Norwegian University of Science and Technology, 7491 Trondheim, Norway
[3]UMR CNRS 6027, IRDL, ENI Brest, 29200 Brest, France

Corresponding author: Thor I. Fossen (thor.fossen@ntnu.no)

This work was supported in part by the ISblue Project, Interdisciplinary Graduate School for the Blue Planet, under Grant ANR-17-EURE-0015; and in part by French Government Grant through the Program ''Investissements d'Avenir.'' The work of Loïck Degorre was supported in part by Région Bretagne under Grant 0311/COH20007/00019559, and in part by Brest Métropole.

ABSTRACT This work presents a novel method for 3-D path-following and path-tracking of Autonomous Underwater Vehicles (AUVs) using the concept of a Virtual Reference Point (VRP) and a kinematic guidance principle. The origins of the along-, cross- and vertical-track errors are proven globally exponentially stable (GES) using Lyapunov stability analysis. The kinematic guidance law exploits the design flexibility of a user-defined VRP in conjunction with a feedback linearizing controller. In addition, a novel concept called the Handy Matrix is introduced and applied to shape the kinematic equations such that the AUV's non-actuated degrees of freedom (DOFs) can be controlled in a 3-D path-following scenario. The case study considers the Remus 100, a torpedo-shaped underactuated AUV, performing a 3-D path-following maneuver. The computer simulations show that the kinematic guidance law shows excellent tracking performance and stability even in the presence of ocean currents and white measurement noise.

INDEX TERMS Autonomous underwater vehicles, guidance systems, kinematic control, path following, underactuated system.

I. INTRODUCTION

The rapidly growing number of new marine applications like monitoring and inspection of offshore power plants, subsea infrastructure, and fish farms raise the need for cheap and performant Autonomous Underwater Vehicles (AUVs). One of the main tasks for these vehicles is path following and path tracking. In path following, the vehicle follows predefined lines or curve segments between waypoints without time constraint; Samson [1], Micaelli and Samson [2]. Several solutions to the path-following problem have been proposed over the years, including utilizing the *Serret-Frenet* frame; Rouchon and Rudolph [3], Lapierre et al. [4], Lapierre and Jouvencel [5]. Another formalism, using a parametrized path frame centered on a virtual particle (Breivik and Fossen [6]), is the basis for this article. The main idea is that the vehicle tracks a virtual path particle evolving along a 3-D path at a controlled speed. Consequently, path-following is achieved by minimizing the cross-, along-, and vertical-track errors between the path particle and the particle representing the vehicle.

A. THE REMUS 100 AUV

The most common AUVs are underactuated for better cost efficiency and autonomy, meaning they have less than six actuated degrees of freedom (DOFs). The AUV studied in this article is the Remus 100 AUV shown in Figure 1, developed by Hydroid, Inc., a spin-off company from the Woods Hole Oceanographic Institution. The Remus 100 is a torpedo-shaped vehicle controlled by a propeller, a stern

The associate editor coordinating the review of this manuscript and approving it for publication was Huiyan Zhang.

FIGURE 1. The Remus 100 AUV at the NTNU applied underwater robotics laboratory (AUR-Lab); see https://www.ntnu.no/aur-lab.

rudder, and a stern dive plane. Torpedo-shaped vehicles are usually actuated in *surge, pitch*, and *yaw* but lack actuation in the *sway, heave*, and *roll* modes. However, the roll dynamics is naturally stable if the center of gravity (CG) is below the buoyancy (CB) center. This work's control objective is 3-D translational control corresponding to regulating the along-, cross-, and vertical-track errors to zero. Therefore, the Remus 100 AUV has a sufficient number of actuated DOFs, but there is a mismatch; It has one actuated translation and two rotations, while the control objective requires three translations. It is, therefore, said to be *ill-actuated*, and a guidance algorithm – in this work, at the kinematic level – is necessary to transform the control objective to reference signals that match the actuated DOFs.

B. STATE-OF-THE-ART GUIDANCE PRINCIPLES

Many vehicle control systems use proportional Line-of-Sight (LOS) guidance laws for path following, where the proportional gain is typically the inverse of the look-ahead distance. For 2-D path-following problems, the LOS guidance law can mimic the course angle command of an experienced navigator; Healey and Lienard [7], Breivik and Fossen [8]. The LOS guidance law reproduces the behavior of the navigator by calculating the autopilot azimuth and elevation references (alternatively, the course and flight-path angles), minimizing cross- and vertical-track errors. By doing this, pitch and yaw rotations can compensate for the lack of actuation in the sway and heave directions. This method has been applied to marine craft, as discussed by Berge et al. [9], Pettersen and Lefeber [10], Fossen et al. [11], and Breivik and Fossen [6]. A similar approach has been applied to small uncrewed aerial vehicles (UAVs) by Nelson et al. [12, using a vector field surrounding the path to generate course commands. A comparative study of LOS and vector-field guidance laws is found in Caharija et al. [13]. Proportional guidance laws are also used in missile guidance, as discussed in Siouris [14] and Yanushevsky [15]. Several authors have designed model-based predictive control (MPC) LOS guidance laws; Pavlov et al. [16]; Oh and Sun [17]; Liu et al. [18]; Rout and Subudhi [19]. Serret-Frenet frame guidance laws for AUVs are discussed by Encarnacao and Pascoal [20].

When vehicles are exposed to drift forces from winds, waves, and ocean currents, the standard solution is integral LOS (ILOS), as detailed in Børhaug et al. [21]. The ILOS guidance law has seen successful implementation in various applications, including those cited in Caharija et al. [22]. Extensions to path following for curved paths have been explored by Lekkas and Fossen [23]. Adaptive sideslip compensation (Fossen et al. [24]) and the 3-D adaptive LOS (ALOS) guidance law by Fossen and Aguiar [25] are alternatives to the integral state in ILOS. Furthermore, Fossen and Lekkas [26] have derived indirect and direct adaptive control laws for LOS path following. Alternative designs include the reducedorder extended state observer for estimating the crab angle, known as the ELOS guidance law (Liu et al. [27]).

The horizontal-plane LOS guidance principle has been extended to 3-D path-following by adding a second LOS guidance law for altitude/depth control, assuming decoupled motions between horizontal and vertical planes, as seen in Lekkas and Fossen [28] and Caharija [29]. Vadapalli and Mahapatra [30] proposes a decoupled AUV guidance and control strategy based on semi-definite programming. Liu et al. [31] suggests a time-varying look-ahead distance for 3-D adaptive path-following of AUVs, and an extension to 3-D vector field guidance can be found in Yao and Cao [32]. Reinforced learning applied to 3-D path following AUVs is discussed by Havenstrøm et al. [33]. Pelizer et al. [34] has compared several 3-D path-following algorithms for UAVs, and Monte Carlo simulations for analyzing five 3-D path-following algorithms, focusing on their robustness to wind loads and tuning, are presented in Sujit et al. [35]. Comparatively, the method proposed in this work has the advantage of constructing a closed-loop system that is linear and decoupled for the controlled DOF. This is mainly due to the kinematic model-based structure of the guidance principle, which allows for the exact cancellation of the closed-loop coupling terms. This linear framework allows easy and intuitive controller tuning using standard methods for linear systems.

C. VIRTUAL REFERENCE POINT KINEMATIC GUIDANCE PRINCIPLE

This work applies the new kinematic guidance principle introduced in Degorre [36] to solve the kinematic path-following control problem. This is achieved by defining a Virtual Reference Point (VRP) positioned at the vehicle's bow when tracking a particle moving along the path (Alonge et al. [37]). The VRP and its design parameters introduce new kinematic couplings that naturally increase the AUV's stability in a maneuvering situation (Berge et al. [9]).

The kinematic couplings are further exploited when designing a matrix, $\mathcal{H}$, referred to as the *Handy Matrix*. The $\mathcal{H}$ matrix defines the control objective (DOFs to be controlled) and the non-actuated DOFs of the vehicle. It is easy and intuitive to interpret the Handy Matrix when deriving the guidance law; see Algorithm 1 in Appendix. A key observation of the proposed method is that it creates a linear relationship between the output and the control law, which is not true when using classical LOS algorithms. Therefore, the AUV dynamics can be intuitively tailored with state-of-the-art control methods such as Proportional-Integral-Derivative (PID), feedback linearization, or sliding-mode control (SMC). Applications are discussed by

Yoerger and Slotine [38], Cristi et al. [39], Healey and Lienard [7], Elmokadem et al. [40], while a review of SMC applied to AUVs is found in Mat-Noh et al. [41]. The proposed path-following controller is computed in two stages. The velocity references are calculated by the kinematic guidance law in the first stage using the VRP and the $\mathcal{H}$ matrix and then used in a feedback linearizing control law in the second stage. Finally, the computed forces and moments are mapped to actuator commands using control allocation (Johansen and Fossen [42]). Also, thanks to the method's simplified formalism and the algorithm to calculate the Handy Matrix $\mathcal{H}$, this solution can be easily reproduced on other vehicles with different actuation.

D. MAIN CONTRIBUTIONS

A significant contribution of this work is demonstrating that applying a feedback control law to stabilize the VRP offers a simple yet effective solution for the 3-D *path-following* problem. Furthermore, we extend this approach to *path-tracking*. This achievement is facilitated by utilizing a novel concept called the Handy Matrix to shape the kinematic equations. Furthermore, it is demonstrated how the VRP and the Handy Matrix can control the non-actuated DOFs of an AUV in a 3-D path-following scenario. An algorithm for constructing the Handy Matrix is also proposed (Appendix). Notably, this customization can be accomplished regardless of the AUV's model parameters, enabling straightforward and intuitive tuning of the AUV's dynamic behavior in closed loop. Additionally, we prove that the origins of the along-, cross-, and vertical-track errors are globally exponentially stable (GES) using Lyapunov stability theory, ensuring strong convergence and robustness against perturbations.

E. ORGANIZATION OF THE ARTICLE

The paper is organized as follows. In Section II, the kinematic and kinetic equations of the AUV are expressed as a function of the VRP. Then, in Section III, the 3-D path-following problem is defined before introducing the two-stage control design method (Section IV), which includes the algorithm for the Handy Matrix (Appendix). The stability proof and main contributions related to the proof are presented in Section V. Finally, Section VI concludes by showcasing the simulation results, which affirm the method's outstanding efficacy through two case studies involving the Remus 100 AUV in a 3-D path-following scenario.

II. AUV EQUATIONS OF MOTION

The AUV equations of motion are based on the cylinder-shaped model presented in Fossen [43, Ch. 8.4] and the references therein. It is assumed that the hydrodynamic added mass, damping, and hydrostatic coefficients are known. This assumption can be relaxed using an SMC instead of feedback linearization to control the vehicle. The AUV maneuvering model is modified to take the VRP into account according to

$$\dot{\boldsymbol{\eta}}_E = \boldsymbol{J}(\boldsymbol{\eta})\boldsymbol{T}_E\boldsymbol{\nu} \tag{1a}$$

$$\boldsymbol{M}\dot{\boldsymbol{\nu}} + \boldsymbol{C}(\boldsymbol{\nu})\boldsymbol{\nu} + \boldsymbol{D}(\boldsymbol{\nu})\boldsymbol{\nu} + \boldsymbol{g}(\boldsymbol{\eta}) = \boldsymbol{\tau} + \boldsymbol{d} \tag{1b}$$

where $\boldsymbol{d}$ is a nearly constant bounded external disturbance vector due to ocean currents and unmodelled dynamics. Further, $\boldsymbol{\eta}_E = [x, y, z, \phi, \theta, \psi]^\top$ is the generalized position vector expressed in the North-East-Down (NED) frame $\mathcal{R}_0$. The vehicle's generalized velocity vector $\boldsymbol{\nu} = [u, v, w, p, q, r]^\top$ is expressed in the body-fixed frame $\mathcal{R}_B$. The kinematic transformation matrix $\boldsymbol{J}(\boldsymbol{\eta}) = \text{diag}\{\boldsymbol{J}_1(\boldsymbol{\eta}), \boldsymbol{J}_2(\boldsymbol{\eta})\}$ is given by [43, Ch. 2]:

$$\boldsymbol{J}_1(\boldsymbol{\eta}) = \boldsymbol{R}(\boldsymbol{x}_0, \phi)\boldsymbol{R}(\boldsymbol{y}_0, \theta)\boldsymbol{R}(\boldsymbol{z}_0, \psi) \tag{2a}$$

$$\boldsymbol{J}_2(\boldsymbol{\eta}) = \begin{bmatrix} 1 & \sin(\phi)\tan(\theta) & \cos(\phi)\tan(\theta) \\ 0 & \cos(\phi) & -\sin(\phi) \\ 0 & \frac{\sin(\phi)}{\cos(\theta)} & \frac{\cos(\phi)}{\cos(\theta)} \end{bmatrix},$$

$$\theta \neq \pm\frac{\pi}{2} + 2\,n\pi, \ (n = 1, 2, ..N) \tag{2b}$$

where $\boldsymbol{R}(\boldsymbol{\lambda}, \chi)$ is a rotation of angle χ around axis $\boldsymbol{\lambda}$. The matrices $\boldsymbol{M}$, $\boldsymbol{C}(\boldsymbol{\nu})$, and $\boldsymbol{D}(\boldsymbol{\nu})$ represent the rigid-body and hydrodynamic added mass, Coriolis and centripetal forces, and hydrodynamic damping, respectively. The vector $\boldsymbol{g}(\boldsymbol{\eta})$ contains the gravitational and buoyancy terms, while the vector $\boldsymbol{\tau}$ represents the forces and moments generated by the vehicle's actuators. The Remus 100 AUV shown in Figure 1 is equipped with a single propeller, a stern rudder, and a stern diving plane. Hence, it is actuated in *surge, pitch*, and *yaw*. Consequently,

$$\boldsymbol{\tau} = [X,\ 0,\ 0,\ 0,\ M,\ N]^\top \tag{3}$$

where X is the surge force (propeller) and M (stern plane) and N (tail rudder) are the pitch and yaw moments, respectively. The vehicle is naturally stable in roll and pitch because of the restoring moments created by locating the CG below the CB. The shape and actuator configuration of the Remus 100 also suggests that the sway and heave coupling forces due to the control surfaces can be neglected. Finally, the matrix $\boldsymbol{T}_E$ is used to translate the velocity vector from the origin of the body-fixed frame $\mathcal{R}_B$ to an arbitrary VRP specified by the user. Choosing $\boldsymbol{E} = [\epsilon_x,\ \epsilon_y,\ \epsilon_z]^\top$, the transformation matrix becomes

$$\boldsymbol{T}_E := \begin{bmatrix} \mathbb{I}_3 & \boldsymbol{S}_E \\ \boldsymbol{0}_{3\times3} & \mathbb{I}_3 \end{bmatrix} \tag{4}$$

where $\boldsymbol{S}_E$ is the skew-symmetrical matrix defined by

$$\boldsymbol{S}_E := \begin{bmatrix} 0 & \epsilon_z & -\epsilon_y \\ -\epsilon_z & 0 & \epsilon_x \\ \epsilon_y & -\epsilon_x & 0 \end{bmatrix} \tag{5}$$

Hence, if the VRP is located on the centerline in front of the vehicle, $\boldsymbol{E} = [\epsilon_x,\ 0,\ 0]^\top$ and $\epsilon_x > 0$ such that

$$\boldsymbol{T}_E = \begin{bmatrix} 1 & 0 & 0 & 0 & 0 & 0 \\ 0 & 1 & 0 & 0 & 0 & \epsilon_x \\ 0 & 0 & 1 & 0 & -\epsilon_x & 0 \\ 0 & 0 & 0 & 1 & 0 & 0 \\ 0 & 0 & 0 & 0 & 1 & 0 \\ 0 & 0 & 0 & 0 & 0 & 1 \end{bmatrix} \tag{6}$$

III. PROBLEM STATEMENT

This section describes the 3-D path-following problem using the guidance-based path-following principle of Breivik and Fossen [8]. The position $\boldsymbol{p} = [x,\ y,\ z]^\top$ of the vehicle's VRP is expressed in the NED frame, and the position of the virtual particle evolving on the path is denoted by $\boldsymbol{p}_p = [x_p,\ y_p,\ z_p]^\top$. The NED frame is assumed to be an (approximate) inertial frame. Only the 3-D position of the particles is considered. The roll and pitch modes are naturally stable due to metacentric stability. At the same time, the yaw angle is indirectly stabilized by introducing the VRP, typically in front of the vehicle. The geometric path, P, is parametrized by the scalar variable ϖ, which is similar to the curvilinear abscissa of the *Serret-Frenet* frame; Samson [1], Lapierre et al. [4]. This is mathematically equivalent to

$$P = \{\boldsymbol{p} \in \mathbb{R}^3 \ \mid \ \boldsymbol{p} = \boldsymbol{p}_p(\varpi)\ \ \forall\ \varpi \in \mathbb{R}\} \tag{7}$$

A local path frame $\mathcal{R}_p$ centered on $\boldsymbol{p}_p(\varpi)$ is defined such that the $\boldsymbol{x_p}$ axis of $\mathcal{R}_p$ is always tangential to the path. The path frame results from two consecutive rotations of the inertial frame. First, a rotation of angle χ_p (azimuth angle) around the $\boldsymbol{z}_0$ axis and then a rotation of angle ν_p (elevation angle) around the $\boldsymbol{y}$ axis of the intermediate frame thus created. For a given $\boldsymbol{p}_p(\varpi)$, the two angles are

$$\chi_p(\varpi) = \text{atan2}\left(y_p'(\varpi), x_p'(\varpi)\right) \tag{8a}$$

$$\nu_p(\varpi) = \text{atan2}\left(-z_p'(\varpi), \sqrt{x_p'(\varpi)^2 + y_p'(\varpi)^2}\right) \tag{8b}$$

where $\cdot'$ is the derivative operator $\mathrm{d}/\mathrm{d}\varpi$. The two associated rotation matrices are

$$\boldsymbol{R}_{p,z}(\chi_p(\varpi)) = \begin{bmatrix} \cos(\chi_p) & -\sin(\chi_p) & 0 \\ \sin(\chi_p) & \cos(\chi_p) & 0 \\ 0 & 0 & 1 \end{bmatrix} \tag{9a}$$

$$\boldsymbol{R}_{p,y}(\nu_p(\varpi)) = \begin{bmatrix} \cos(\nu_p) & 0 & \sin(\nu_p) \\ 0 & 1 & 0 \\ -\sin(\nu_p) & 0 & \cos(\nu_p) \end{bmatrix} \tag{9b}$$

Hence, the full rotation from the inertial frame to the path frame is

$$\boldsymbol{R}_p(\varpi) = \boldsymbol{R}_{p,z}(\chi_p(\varpi))\boldsymbol{R}_{p,y}(\nu_p(\varpi)) \tag{10}$$

In the subsequent sections, it will be assumed that the path satisfies the following conditions:

A.1 The path is regular, i.e., $\varpi > 0$, $\dot{\varpi} > 0\ \forall\ t > 0$.

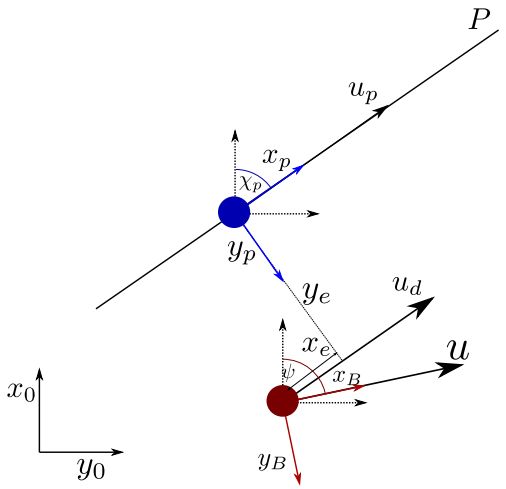

FIGURE 2. Schematic representation of the path-following problem in the horizontal plane. Red: Vehicle VRP, Blue: Virtual path particle.

A.2 The virtual particle always moves tangentially to the path with velocity $\boldsymbol{v}_p = [u_p, 0, 0]^\top$ expressed in the path frame where u_p is the particle velocity.

Remark 1: Note that assuming that the particle always moves forward on the path ($u_p > 0$) is not necessary to prove stability. Some applications could benefit from adapting the path particle's velocity to the vehicle's behavior.

The error between the virtual path particle and the tracking point of the vehicle expressed in the path frame is

$$\boldsymbol{\varepsilon} = \boldsymbol{R}_p^\top(\boldsymbol{p} - \boldsymbol{p}_p(\varpi)) \tag{11}$$

The elements of the error vector $\boldsymbol{\varepsilon} = [x_e,\ y_e,\ z_e]^\top$ are recognized as the *along-track error*, *cross-track error*, and *vertical-track error*, respectively. Next, the desired velocity vector expressed in the path frame $\boldsymbol{v}_d$ is introduced. It represents the velocity of the VRP when moving along the path. The vehicle is expected to travel tangentially to the path, and thus $\boldsymbol{v}_d = [u_d,\ 0,\ 0]^\top$ where the desired surge velocity u_d is a control parameter. With these definitions, 3-D path-following is achieved if the error vector $\boldsymbol{\varepsilon}$ is regulated to zero while the path-particle proceeds along the path with predefined velocity u_p.

IV. VIRTUAL REFERENCE POINT KINEMATIC GUIDANCE LAW

The inner-loop feedback linearizing controller and the path-following guidance law (Degorre [36]) are applied to the Remus 100 AUV as illustrated in Figure 3 where the symbol Σ represents the AUV system dynamics. The kinematic guidance law, including the Handy Matrix, constitutes the outer-loop controller. The two design steps of the control law are outlined below.

A. TWO-STAGE CONTROL DESIGN

For notational convenience, the Coriolis-centripetal, damping, gravity, and buoyancy forces in (1b) are collected into

the vector

$$\boldsymbol{n}(\boldsymbol{\nu}, \boldsymbol{\eta}) := \boldsymbol{C}(\boldsymbol{\nu})\boldsymbol{\nu} + \boldsymbol{D}(\boldsymbol{\nu})\boldsymbol{\nu} + \boldsymbol{g}(\boldsymbol{\eta}) \tag{12}$$

Hence, the inner-loop control system can be designed as a feedback-linearizing controller

$$\boldsymbol{\tau} = \boldsymbol{M}\left(\dot{\boldsymbol{\nu}}_c + \boldsymbol{K}(\boldsymbol{\nu}_c - \boldsymbol{\nu})\right) + \boldsymbol{n}(\boldsymbol{\nu}, \boldsymbol{\eta}) \tag{13}$$

where $\boldsymbol{K}$ is a diagonal positive definite gain matrix representing the convergence rate of the error dynamics. Consequently, $(\dot{\boldsymbol{\nu}} - \dot{\boldsymbol{\nu}}_c) = -\boldsymbol{K}(\boldsymbol{\nu} - \boldsymbol{\nu}_c)$, and the linear velocity vector $\boldsymbol{\nu}$ converges exponentially to $\boldsymbol{\nu}_c$.

The second stage uses the Handy Matrix to calculate the kinematic guidance law's velocity reference signal $\boldsymbol{\nu}_c := \mathcal{H}\boldsymbol{\nu}$. Furthermore, let $\boldsymbol{\lambda}$ denote a virtual controller applied to (1a) such that $\dot{\boldsymbol{\eta}}_E = \boldsymbol{J}(\boldsymbol{\eta})\boldsymbol{T}_E\boldsymbol{\nu} \equiv \boldsymbol{\lambda}$. Consequently,

$$\boldsymbol{\nu}_c = \mathcal{H}\boldsymbol{T}_E^{-1}\boldsymbol{J}(\boldsymbol{\eta})^{-1}\boldsymbol{\lambda} \tag{14}$$

The virtual control law is chosen as a PI controller with feedforward from the desired velocity vector $\boldsymbol{v}_d$ expressed in NED. This is mathematically equivalent to

$$\boldsymbol{\lambda} = [\boldsymbol{\lambda}_1^\top,\ 0,\ 0,\ 0]^\top \tag{15a}$$

$$\boldsymbol{\lambda}_1 = \boldsymbol{R}_p\left(\boldsymbol{v}_d - \boldsymbol{K}_p\boldsymbol{\varepsilon} - \boldsymbol{K}_i\int_0^t \boldsymbol{\varepsilon}(\sigma)\mathrm{d}\sigma\right) \tag{15b}$$

where $\boldsymbol{K}_p > 0$ and $\boldsymbol{K}_i \geq 0$ are positive definite proportional and integral gain matrices, respectively. The optional integral term can compensate for nearly constant drift due to ocean currents and unmodelled dynamics. Note that the virtual controller $\boldsymbol{\lambda}_1$ is only applied to the positions.

B. CONTROLLING NON-ACTUATED DEGREES OF FREEDOM WITH THE HANDY MATRIX

The design matrix, denoted as $\mathcal{H}$, is called the *Handy Matrix* and is derived in Appendix (Degorre [36]). Its non-diagonal structure plays a crucial role in shaping the expected behavior of the kinematic guidance law. The non-zero elements of this matrix are strategically utilized to harness the kinematic couplings present in the AUV model, thereby enabling control over the non-actuated DOFs. Notably, in this context, $\mathcal{H}$ facilitates the computation of pitch and yaw velocity references. These calculations are instrumental in compensating for the absence of heave and sway actuation, respectively. From Appendix, it follows that $\boldsymbol{\nu}_c := \mathcal{H}\boldsymbol{\nu}$ where the Handy Matrix can be expressed by

$$\mathcal{H} = \begin{bmatrix} 1 & 0 & 0 & 0\ 0\ 0 \\ 0 & 0 & 0 & 0\ 0\ 0 \\ 0 & 0 & 0 & 0\ 0\ 0 \\ 0 & 0 & 0 & 1\ 0\ 0 \\ 0 & 0 & -1/\epsilon_x & 0\ 1\ 0 \\ 0 & 1/\epsilon_x & 0 & 0\ 0\ 1 \end{bmatrix} \tag{16}$$

if $\boldsymbol{E} = [\epsilon_x,\ 0,\ 0]^\top$. Due to the off-diagonal elements in the fifth and sixth rows of the Handy Matrix, the pitch velocity reference (as indicated in the fifth row of $\boldsymbol{\nu}_c$) becomes dependent on the heave tracking error at the VRP. Similarly, the yaw velocity reference (in the sixth row of $\boldsymbol{\nu}_c$) is influenced by the sway tracking error at the VRP. This configuration allows for precise control of the VRP velocity through the vehicle's actuated rotations. The algorithm employed for constructing the matrix $\mathcal{H}$ is outlined in Appendix, and a more detailed explanation of its development is available in Degorre [36]. It should be noted that this method does not control the vehicle's attitude. However, due to the inherent rotational stability the VRP provides, the vehicle naturally tends to align with the VRP's velocity vector, thus achieving tangential stabilization to the path with and without environmental disturbances. Furthermore, as the vehicle's attitude is not a critical component of the task requirements (the AUV is metacentric stable in roll and pitch), it can remain uncontrolled, provided it does not adversely affect the other controlled DOFs, as demonstrated in Degorre [36]. The feedback linearizing controller (13) guarantees convergence of the vehicle velocity $\boldsymbol{\nu}$ towards the reference velocity $\boldsymbol{\nu}_c$. Hence, if $\boldsymbol{\nu} \equiv \boldsymbol{\nu}_c$ the kinematic equation (1a) becomes

$$\begin{aligned} \dot{\boldsymbol{\eta}}_E &= \boldsymbol{J}(\boldsymbol{\eta})\boldsymbol{T}_E\boldsymbol{\nu}_c \\ &= \boldsymbol{J}(\boldsymbol{\eta})\boldsymbol{T}_E\mathcal{H}\boldsymbol{T}_E^{-1}\boldsymbol{J}(\boldsymbol{\eta})^{-1}\boldsymbol{\lambda} \end{aligned} \tag{17}$$

where $\dot{\boldsymbol{\eta}}_E = [\dot{\boldsymbol{p}}^\top,\ \dot{\phi},\ \dot{\theta},\ \dot{\psi}]^\top$ and

$$\boldsymbol{T}_E\mathcal{H}\boldsymbol{T}_E^{-1} = \begin{bmatrix} 1 & 0 & 0 & 0\ 0\ 0 \\ 0 & 1 & 0 & 0\ 0\ 0 \\ 0 & 0 & 1 & 0\ 0\ 0 \\ 0 & 0 & 0 & 1\ 0\ 0 \\ 0 & 0 & -1/\epsilon_x & 0\ 0\ 0 \\ 0 & 1/\epsilon_x & 0 & 0\ 0\ 0 \end{bmatrix} \tag{18}$$

Hence, the first three differential equations in (17) with the control law (15a)–(15b) becomes

$$\dot{\boldsymbol{p}} = \boldsymbol{\lambda}_1 \tag{19}$$

Equation (19) illustrates one of the key benefits of the proposed method. The $\mathcal{H}$ matrix transforms the kinematic equations to a linear decoupled system (19) with control input $\boldsymbol{\lambda}_1$. This customization is achievable independently of the system's parameters. Furthermore, the linear relationship between the VRP's velocity vector expressed in NED and the control law facilitates straightforward and intuitive tuning of the system's behavior.

V. LYAPUNOV STABILITY ANALYSIS

The stability of the kinematic guidance law and path-following controller is proven using the Lyapunov theory. Consider the Lyapunov function candidate (LFC)

$$V = \frac{1}{2}\boldsymbol{\varepsilon}^\top\boldsymbol{\varepsilon} + \frac{1}{2}\boldsymbol{z}_{\text{int}}^\top\boldsymbol{K}_i\boldsymbol{z}_{\text{int}} \tag{20}$$

where $\dot{\boldsymbol{z}}_{\text{int}} = \boldsymbol{\varepsilon}$ is the integral state in the control law (15b). The time derivative of the error vector expressed in the path

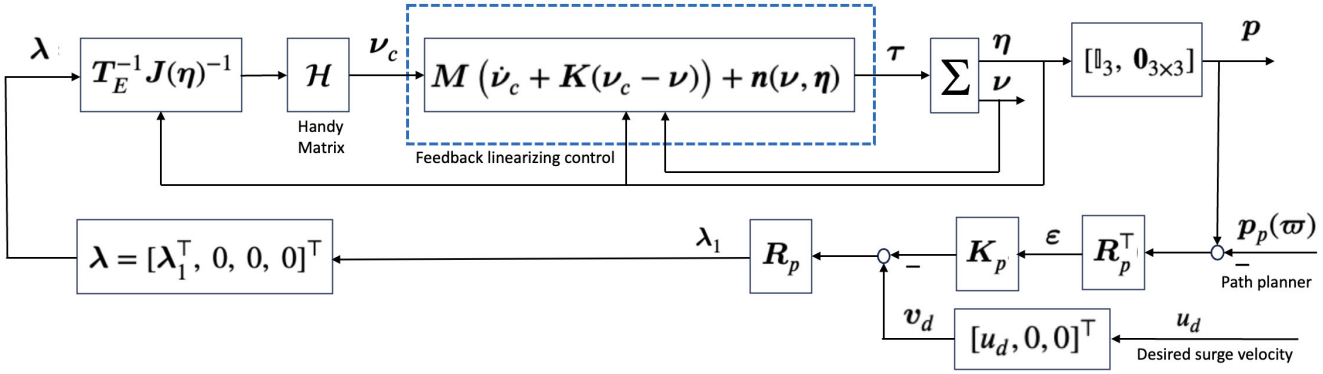

FIGURE 3. Block diagram showing the feedback linearizing controller (inner loop) and a proportional kinematic guidance law ($K_p > 0$ and $K_i = \mathbf{0}_{3\times3}$) with the Handy Matrix (outer loop). The symbol Σ denotes the AUV.

frame is

$$\begin{aligned}\dot{\varepsilon} &= \dot{\boldsymbol{R}}_p^\top(\boldsymbol{p} - \boldsymbol{p}_p) + \boldsymbol{R}_p^\top(\dot{\boldsymbol{p}} - \dot{\boldsymbol{p}}_p) \\ &= \boldsymbol{S}_p^\top \boldsymbol{R}_p^\top(\boldsymbol{p} - \boldsymbol{p}_p) + \boldsymbol{R}_p^\top(\dot{\boldsymbol{p}} - \dot{\boldsymbol{p}}_p) \\ &= \boldsymbol{S}_p^\top \varepsilon + \boldsymbol{R}_p^\top(\dot{\boldsymbol{p}} - \dot{\boldsymbol{p}}_p)\end{aligned} \tag{21}$$

where $\boldsymbol{S}_p = -\boldsymbol{S}_p^\top$ is recognized as the skew-symmetric matrix

$$\boldsymbol{S}_p = \begin{bmatrix} 0 & \dot{\chi}_p \cos(\nu_p) & -\dot{\nu}_p \\ -\dot{\chi}_p \cos(\nu_p) & 0 & -\dot{\chi}_p \sin(\nu_p) \\ \dot{\nu}_p & \dot{\chi}_p \sin(\nu_p) & 0 \end{bmatrix} \tag{22}$$

Hence, the time derivative of the LFC along the trajectories of ε and $\boldsymbol{z}_{\text{int}}$ becomes

$$\begin{aligned}\dot{V} &= \varepsilon^\top \left(\boldsymbol{S}_p^\top \varepsilon + \boldsymbol{R}_p^\top(\dot{\boldsymbol{p}} - \dot{\boldsymbol{p}}_p)\right) + \varepsilon^\top \boldsymbol{K}_i \boldsymbol{z}_{\text{int}} \\ &= \varepsilon^\top \left(\boldsymbol{R}_p^\top(\dot{\boldsymbol{p}} - \dot{\boldsymbol{p}}_p) + \boldsymbol{K}_i \boldsymbol{z}_{\text{int}}\right)\end{aligned} \tag{23}$$

where we have exploited that $\varepsilon^\top \boldsymbol{S}_p \varepsilon \equiv 0$. From (19) it follows that $\dot{\boldsymbol{p}} = \boldsymbol{\lambda}_1$ with $\boldsymbol{\lambda}_1$ defined in (15b). Hence, $\dot{V}$ becomes

$$\begin{aligned}\dot{V} &= \varepsilon^\top \left(\boldsymbol{R}_p^\top(\boldsymbol{\lambda}_1 - \dot{\boldsymbol{p}}_p) + \boldsymbol{K}_i \boldsymbol{z}_{\text{int}}\right) \\ &= \varepsilon^\top \left(\boldsymbol{R}_p^\top \left(\boldsymbol{R}_p \left(\boldsymbol{v}_d - \boldsymbol{K}_p \varepsilon - \boldsymbol{K}_i \boldsymbol{z}_{\text{int}}\right) - \dot{\boldsymbol{p}}_p\right) + \boldsymbol{K}_i \boldsymbol{z}_{\text{int}}\right)\end{aligned} \tag{24}$$

Note that the virtual path particle is constrained to the path with its velocity vector expressed in the inertial frame according to

$$\dot{\boldsymbol{p}}_p = \boldsymbol{R}_p \boldsymbol{v}_p = \boldsymbol{R}_p \left[u_p,\ 0,\ 0\right]^\top \tag{25}$$

This implies that (24) can be written as

$$\begin{aligned}\dot{V} &= \varepsilon^\top \left(\boldsymbol{v}_d - \boldsymbol{K}_p \varepsilon - \boldsymbol{v}_p\right) \\ &= -\varepsilon^\top \boldsymbol{K}_p \varepsilon + \left(u_d - u_p\right) x_e\end{aligned} \tag{26}$$

- **Path following** is obtained by choosing the particle velocity equal to the desired surge velocity

$$u_p = u_d \tag{27}$$

In this case, the AUV operator specifies the desired surge velocity u_d beforehand.

- **Path tracking** is obtained by choosing the vehicle's desired surge velocity to catch up with an arbitrary particle velocity. To do so, the desired surge velocity of the vehicle is chosen as

$$u_d = u_p - k_x x_e \tag{28}$$

where $k_x \geq 0$ is an optional feedback gain. Here, the particle velocity u_p is specified to satisfy a dynamic task. In both cases, the path variable propagates according to

$$\dot{\varpi} = \frac{u_p}{\sqrt{x_p'(\varpi)^2 + y_p'(\varpi)^2 + z_p'(\varpi)^2}} \tag{29}$$

The formula (28) is particularly interesting since it allows an operator to choose the whole system's behavior (vehicle and path particle) by tuning only the particle velocity u_p and the control parameters. A typical application is formation control, where several vehicles and particle velocities are used to define the formation of vehicles.

Since the tracking error (21) is a *nonautonomous* differential equation, the stability analysis is more complicated when including integral action:

$$\begin{aligned}\boldsymbol{K}_i \equiv \mathbf{0}_{3\times3} \implies & V = \frac{1}{2}\varepsilon^\top \varepsilon > 0, \\ & \dot{V} = -\varepsilon^\top \boldsymbol{K}_p \varepsilon - k_x x_e^2 < 0 \\ & \text{(GES)} \\ \boldsymbol{K}_i > 0 \implies & V = \frac{1}{2}\varepsilon^\top \varepsilon + \frac{1}{2}\boldsymbol{z}_{\text{int}}^\top \boldsymbol{K}_i \boldsymbol{z}_{\text{int}} > 0, \\ & \dot{V} = -\varepsilon^\top \boldsymbol{K}_p \varepsilon - k_x x_e^2 \leq 0 \\ & \text{(Globally convergent)}\end{aligned}$$

Consequently, the equilibrium $\varepsilon = \mathbf{0}$ is GES when $\boldsymbol{K}_i \equiv \mathbf{0}_{3\times3}$ since the integral state can be omitted in the analysis. If integral action is included ($\boldsymbol{K}_i > 0$), the conditions for GES (Khalil [44, Theorem 4.5]) are violated, since the state vector will be $\boldsymbol{x} = [\varepsilon^\top,\ \boldsymbol{z}_{\text{int}}^\top]^\top$. Then, $V = (1/2)\boldsymbol{x}^\top \boldsymbol{P} \boldsymbol{x}$ and

$\dot{V} = -\boldsymbol{x}^\top \boldsymbol{Q}\boldsymbol{x}$ where $\boldsymbol{P} = \text{diag}\{\mathbb{I}_3, \boldsymbol{K}_i\} > 0$ and $\boldsymbol{Q} = \text{diag}\{\boldsymbol{K}_p + \text{diag}\{k_x, 0, 0\}, \boldsymbol{0}_{3\times 3}\} \geq 0$. However, boundedness of ε and $\boldsymbol{z}_{\text{int}}$ follows from $V > 0$ and $\dot{V} \leq 0$, which again implies that $\ddot{V}$ is bounded. Hence, $\dot{V}$ is uniformly continuous. This allows us to conclude from Barbălat's lemma (Barbălat [45]) that $\dot{V} \to 0$, and thus $\varepsilon \to 0$.

VI. SIMULATION RESULTS

The control strategy developed in Section IV is applied to simulate a high-fidelity model of the Remus 100 AUV. The computer simulations are performed in Matlab using the MSS toolbox (Fossen and Perez [46]) and the `remus100.m` AUV model. The experiments are conducted with a simulated measurement noise of standard deviation 0.1 m for the position measurements and 0.01 rad for the orientations. The parametrized path $\boldsymbol{p}_p(\varpi)$ expressed in NED is defined as 3-D straight lines joining fixed waypoints. The path particle velocity is $u_p = u_d = 2.0\,\text{m s}^{-1}$.

A control allocation algorithm calculates the propeller speed n, rudder deflection angle δ_r, and dive-plane deflection angle δ_s. This is achieved by using

$$n = \text{sign}(X)\sqrt{\frac{|X|}{\rho D^4 K_T(0)}}$$

$$\delta_s = \frac{M}{\frac{1}{2}\rho U_v^2 A_s C_{L_{\delta_s}}}$$

$$\delta_r = \frac{N}{\frac{1}{2}\rho U_h^2 A_r C_{L_{\delta_r}}}$$

where X, M, and N are the first, fifth, and sixth elements of the control vector $\boldsymbol{\tau}$ given by (3). Furthermore, ρ is the density of the water, D is the propeller diameter, $K_T(0)$ is the propeller thrust coefficient at zero advance number, $U_h = (u^2 + v^2)^{1/2}$ and $U_v = (u^2 + w^2)^{1/2}$ are the horizontal and vertical speed components, A_s and A_r are the stern-plane and rudder areas, and $C_{L_{\delta_s}}$ and $C_{L_{\delta_r}}$ are the stern-plane and rudder lift coefficients (Fossen [43, Section 9.7]).

Consider a straight-line segment given by two waypoints (x_i, y_i, z_i) and $(x_{i+1}, y_{i+1}, z_{i+1})$ expressed in NED. Switching between the waypoints is important when implementing straight-line path following control systems. The next waypoint $(x_{i+1}, y_{i+1}, z_{i+1})$ is selected based on whether or not the VRP lies within a sphere of acceptance with radius R around $(x_{i+1}, y_{i+1}, z_{i+1})$. In other words, if the vehicle's position (x, y, z) at time t satisfies

$$(x_{i+1} - x)^2 + (y_{i+1} - y)^2 + (z_{i+1} - z)^2 \leq R^2 \tag{30}$$

the next waypoint $(x_{i+1}^n, y_{i+1}^n, z_{i+1}^n)$ is selected.

A. SIMULATIONS WHEN NO OCEAN CURRENTS EXIST (IDEAL CASE)

In this experiment, the vehicle is initially positioned with a 2 m error along the $\boldsymbol{y}_0$ axis to demonstrate active convergence under ideal conditions. The integral term is not included in the control law (15b). Consequently, we choose $\boldsymbol{K}_i \equiv \boldsymbol{0}_{3\times 3}$. The tracking point and virtual particle positions are illustrated in Figure 4, superimposed throughout the experiment for a simultaneous course- and depth-changing maneuver. Figure 5 indicates that the initial cross-track error converges to zero. A slight vertical-track steady-state error appears during the diving phase (20 s to 150 s) due to actuator saturation. The vehicle's sudden acceleration at the start causes slight oscillations in the along- and vertical-track errors, stabilizing when the vehicle's tracking point catches up with the virtual particle. These oscillations are also observable in the pitch angle, as shown in Figure 6. Furthermore, Figure 6 demonstrates that the AUV aligns with the path between turns and consistently remains tangential to the $\boldsymbol{x_p}$ axis of the path frame.

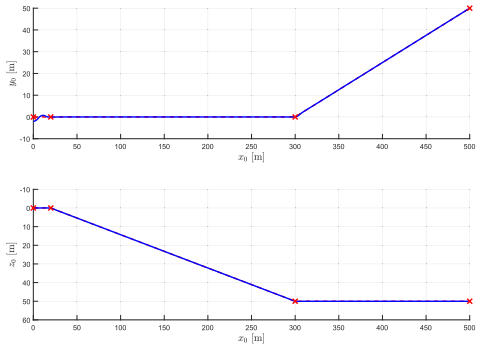

FIGURE 4. Position of the AUV's tracking point (Indicated in Blue) when no ocean currents exist, projected in the (x_0, y_0) horizontal plane (top) and in the (x_0, z_0) vertical plane (bottom). Dashed Red Line: Trajectory of the virtual particle for comparison, Red Crosses: Waypoints.

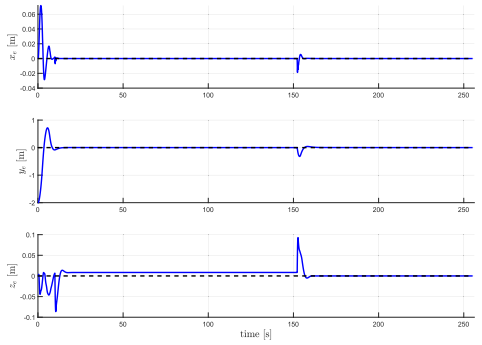

FIGURE 5. The along-, cross-, and vertical-track errors (x_e, y_e, z_e) over time are shown for a scenario with no ocean currents and an initial cross-track error (y_e) of 2m. The dotted line represents a minor offset in the vertical-track error (z_e) due to dive-plane saturation during the steep descent from 0 to 50m.

B. SIMULATIONS WITH NEARLY CONSTANT OCEAN CURRENTS

In this experiment, the AUV is exposed to a $0.5\,\text{m s}^{-1}$ ocean current aligned with the $\boldsymbol{y}_0$ axis. The integral term is included in the control law (15b) to compensate for external disturbances by choosing $\boldsymbol{K}_i > 0$. Figure 7 demonstrates that the path-following performance remains effective despite external disturbances and measurement noise. However,

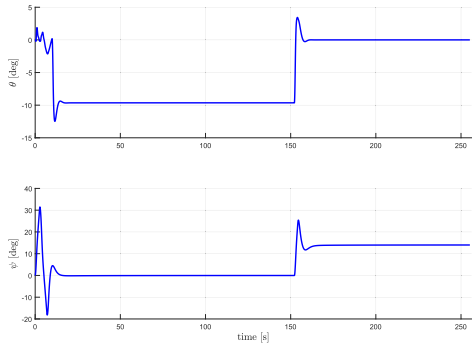

FIGURE 6. Pitch (top) and yaw (bottom) angles of the AUV with no ocean currents.

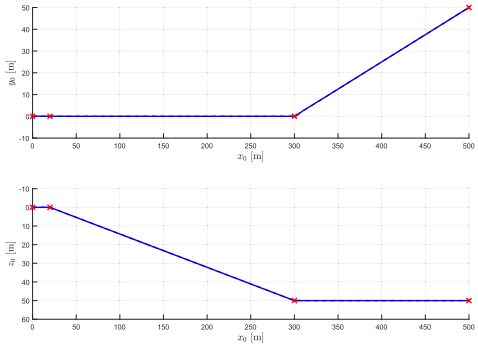

FIGURE 7. Position of the AUV's tracking point (Indicated in Blue) under the influence of ocean currents, projected in the (x_0, y_0) horizontal plane (top) and the (x_0, z_0) vertical plane (bottom). Dashed Red Line: Trajectory of the virtual particle for comparison, Red Crosses: Waypoints.

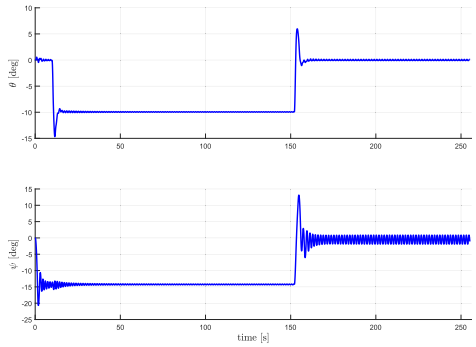

FIGURE 8. Pitch (top) and yaw (bottom) angles of the AUV under the influence of ocean currents. The stochastic ocean current causes the oscillation in the heading angle ψ.

Figure 8 reveals a discrepancy: the yaw angle equilibrium assumed by the AUV between the turns is different from the azimuth angle of the path, a phenomenon known as side-slipping. When subjected to transverse ocean currents, the AUV does not maintain tangential alignment with the path but instead reaches a different equilibrium state known as the flight-path angle. This is the expected behavior of an AUV exposed to drift forces. The course and flight-path angles of an AUV describe the actual direction in which the AUV is moving relative to the Earth, while the yaw and pitch angles represent the orientation of the AUV's body during path following. Additionally, Figure 9 indicates

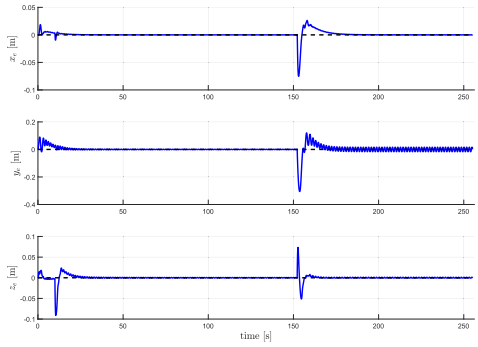

FIGURE 9. Along-, cross-, and vertical-track errors (x_e, y_e, z_e) versus time under the influence of ocean currents. All steady-state errors are compensated by integral action. The stochastic ocean current causes the oscillation in the cross-track error y_e.

that path-tracking errors are effectively mitigated despite non-zero drift forces due to ocean currents. Although the system's robustness to external disturbances has not been formally validated, the cascade structure of the controller, integral action, and the implementation of the VRP ahead of the AUV bolster confidence in its stability and performance under environmental disturbances.

VII. CONCLUSION

In conclusion, this work introduces a novel approach to achieving 3-D path following for Autonomous Underwater Vehicles (AUVs) using a Virtual Reference Point (VRP) and a kinematic guidance principle. The origins of the along-, cross- and vertical-track errors were proven globally exponentially stable (GES) using Lyapunov stability analysis. The kinematic guidance law capitalizes on the flexibility of a user-defined VRP coupled with a feedback linearizing controller. This controller can be replaced by a PID or sliding-mode controller, according to the user's preference. Furthermore, we introduce the innovative concept of the Handy Matrix, which shapes the kinematic equations, enabling control over the AUV's non-actuated degrees of freedom (DOFs) in 3-D path-following and path-tracking scenarios in a linear and decoupled fashion.

Our case study, featuring the Remus 100, a torpedo-shaped underactuated AUV, showcases the effectiveness and stability of the kinematic guidance law in challenging conditions, including ocean currents and measurement noise. These results highlight the guidance principle and control law's excellent performance during simulation tests.

A virtual tracking point and cascaded control structure naturally enhance the system's stability. A significant advantage of the kinematic guidance law and the Handy Matrix lies in its intuitive behavior customization, achieved through the linear relationship between the VRP's velocity and the control input. Beyond the context of AUV path following and path tracking, this work has the potential to extend its applicability to other scenarios, such as leader-follower configurations, where the leader can serve as the target instead of the virtual path particle in the formation control scenarios.

APPENDIX
ALGORITHM FOR CONSTRUCTION OF THE HANDY MATRIX $\mathcal{H}$

The algorithm for constructing the Handy Matrix $\mathcal{H}$ matrix takes three configuration inputs:

1) The position of the tracking point. If $\boldsymbol{E} = [\epsilon_x,\ 0,\ 0]^\top$ the VRP is chosen at a distance ϵ_x in front of the body-fixed coordinate origin.
2) A vector defining the controlled DOFs at the VRP. If $\boldsymbol{h}_E = [1,\ 1,\ 1,\ 0,\ 0,\ 0]^\top$, the three position coordinates of the AUV are controlled and this defines the path-following control objective.
3) A vector defining the actuated DOFs with respect to the body-fixed coordinate origin. If $\boldsymbol{h}_{O_B} = [1,\ 0,\ 0,\ 0,\ 1,\ 1]^\top$ the AUV is actuated in the *surge, pitch*, and *yaw* directions.

Let $\boldsymbol{x} = [x_1,\ x_2,\ x_3]^\top$. The skew-symmetrical matrix $\boldsymbol{S}(\boldsymbol{x})$ is defined by

$$\boldsymbol{S}(\boldsymbol{x}) := \begin{bmatrix} 0 & x_3 & -x_2 \\ -x_3 & 0 & x_1 \\ x_2 & -x_1 & 0 \end{bmatrix} \tag{31}$$

Hence, the algorithm for the computation of the Handy Matrix becomes (Degorre [36])

Algorithm 1 Calculation of the Handy Matrix $\mathcal{H}$

$\mathcal{H} \leftarrow \mathbb{I}_6$
$\boldsymbol{e} \leftarrow [\epsilon_x\ 0\ 0]^\top$
$\boldsymbol{\epsilon} \leftarrow [0\ 0\ 0]^\top$
for $k = 1 : 3$
  if $\boldsymbol{e}(k) \neq 0$
    $\boldsymbol{\epsilon}(k) \leftarrow 1/\boldsymbol{e}(k)$
$\boldsymbol{\Sigma} \leftarrow \boldsymbol{S}(\boldsymbol{\epsilon})$
for $i = 3 : 6$
  if $\boldsymbol{h}_{O_B}(i) = 1 and \boldsymbol{h}_E(i) = 0$
    for $j = 1 : 3$
      if $\boldsymbol{h}_E(j) = 1 and \boldsymbol{h}_{O_B}(j) = 0 and j \neq i - 3$
        $\mathcal{H}(i, j) \leftarrow \Sigma(i - 3, j)$
        $\mathcal{H}(j, :) \leftarrow 0$

ACKNOWLEDGMENT

The authors acknowledge support from the Norwegian University of Science and Technology (NTNU) for covering the open access publication fees of this article.

REFERENCES

[1] C. Samson, "Path following and time-varying feedback stabilization of a wheeled mobile robot," in *Proc. Int. Conf. Control, Autom., Robot. Vis.*, 1992, pp. 1–14.
[2] A. Micaelli and C. Samson, "Trajectory tracking for unicycle-type and two-steering wheels mobile robots," Centre Inria d'Université Côte d'Azur, Sophia Antipolis, France, Res. Rep. RR-2097, 1993.
[3] P. Rouchon and J. Rudolph, "Invariant tracking and stabilization: Problem formulation and examples," in *Stability and Stabilization of Nonlinear Systems*. London, U.K.: Springer, 1999, pp. 261–273.
[4] L. Lapierre, D. Soetanto, and A. Pascoal, "Nonlinear path following with applications to the control of autonomous underwater vehicles," in *Proc. 42nd IEEE Int. Conf. Decis. Control*, vol. 2, Sep. 2003, pp. 1256–1261.
[5] L. Lapierre and B. Jouvencel, "Robust nonlinear path-following control of an AUV," *IEEE J. Ocean. Eng.*, vol. 33, no. 2, pp. 89–102, Apr. 2008.
[6] M. Breivik and T. I. Fossen, "Guidance laws for autonomous underwater vehicles," in *Underwater Vehicles*. London, U.K.: IntechOpen, 2009.
[7] A. J. Healey and D. Lienard, "Multivariable sliding mode control for autonomous diving and steering of unmanned underwater vehicles," *IEEE J. Ocean. Eng.*, vol. 18, no. 3, pp. 327–339, Jul. 1993.
[8] M. Breivik and T. I. Fossen, "Principles of guidance-based path following in 2D and 3D," in *Proc. 44th IEEE Conf. Decis. Control*, Oct. 2005, pp. 627–634.
[9] S. P. Berge, K. Ohtsu, and T. I. Fossen, "Nonlinear control of ships minimizing the position tracking errors," *IFAC Proc. Volumes*, vol. 31, no. 30, pp. 129–134, Oct. 1998.
[10] K. Y. Pettersen and E. Lefeber, "Way-point tracking control of ships," in *Proc. 40th IEEE Conf. Decis. Control*, vol. 1, Jul. 2001, pp. 940–945.
[11] T. I. Fossen, M. Breivik, and R. Skjetne, "Line-of-sight path following of underactuated marine craft," *IFAC Proc. Volumes*, vol. 36, no. 21, pp. 211–216, Sep. 2003.
[12] D. R. Nelson, D. B. Barber, T. W. McLain, and R. W. Beard, "Vector field path following for miniature air vehicles," *IEEE Trans. Robot.*, vol. 23, no. 3, pp. 519–529, Jun. 2007.
[13] W. Caharija, K. Y. Pettersen, P. Calado, and J. Braga, "A comparison between the ILOS guidance and the vector field guidance," *IFAC-PapersOnLine*, vol. 48, no. 16, pp. 89–94, 2015.
[14] G. M. Siouris, *Missile Guidance and Control Systems*. Berlin, Germany: Springer, 2010.
[15] R. Yanushevsky, *Guidance of Unmanned Aerial Vehicles*. Boca Raton, FL, USA: CRC Press, 2011.
[16] A. Pavlov, H. Nordahl, and M. Breivik, "MPC-based optimal path following for underactuated vessels," *IFAC Proc. Volumes*, vol. 42, no. 18, pp. 340–345, 2009.
[17] S.-R. Oh and J. Sun, "Path following of underactuated marine surface vessels using line-of-sight based model predictive control," *Ocean Eng.*, vol. 37, nos. 2–3, pp. 289–295, Feb. 2010.
[18] C. Liu, J. Sun, and Z. Zou, "Integrated line of sight and model predictive control for path following and roll motion control using rudder," *J. Ship Res.*, vol. 59, no. 2, pp. 99–112, Jun. 2015.
[19] R. Rout and B. Subudhi, "Design of line-of-sight guidance law and a constrained optimal controller for an autonomous underwater vehicle," *IEEE Trans. Circuits Syst. II, Exp. Briefs*, vol. 68, no. 1, pp. 416–420, Jan. 2021.
[20] P. Encarnacao and A. Pascoal, "3D path following for autonomous underwater vehicle," in *Proc. 39th IEEE Conf. Decis. Control*, vol. 3, Oct. 2000, pp. 2977–2982.
[21] E. Borhaug, A. Pavlov, and K. Y. Pettersen, "Integral LOS control for path following of underactuated marine surface vessels in the presence of constant ocean currents," in *Proc. 47th IEEE Conf. Decis. Control*, Oct. 2008, pp. 4984–4991.
[22] W. Caharija, K. Y. Pettersen, M. Bibuli, P. Calado, E. Zereik, J. Braga, J. T. Gravdahl, A. J. Sørensen, M. Milovanovic, and G. Bruzzone, "Integral line-of-sight guidance and control of underactuated marine vehicles: Theory, simulations, and experiments," *IEEE Trans. Control Syst. Technol.*, vol. 24, no. 5, pp. 1623–1642, Sep. 2016.
[23] A. M. Lekkas and T. I. Fossen, "Integral LOS path following for curved paths based on a monotone cubic Hermite spline parametrization," *IEEE Trans. Control Syst. Technol.*, vol. 22, no. 6, pp. 2287–2301, Nov. 2014.
[24] T. I. Fossen, K. Y. Pettersen, and R. Galeazzi, "Line-of-sight path following for Dubins paths with adaptive sideslip compensation of drift forces," *IEEE Trans. Control Syst. Technol.*, vol. 23, no. 2, pp. 820–827, Mar. 2015.
[25] T. I. Fossen and A. P. Aguiar, "A uniform semiglobal exponential stable adaptive line-of-sight (ALOS) guidance law for 3-D path following," *Automatica*, vol. 163, May 2024, Art. no. 111556.
[26] T. I. Fossen and A. M. Lekkas, "Direct and indirect adaptive integral line-of-sight path-following controllers for marine craft exposed to ocean currents," *Int. J. Adapt. Control Signal Process.*, vol. 31, no. 4, pp. 445–463, Apr. 2017.
[27] L. Liu, D. Wang, and Z. Peng, "ESO-based line-of-sight guidance law for path following of underactuated marine surface vehicles with exact sideslip compensation," *IEEE J. Ocean. Eng.*, vol. 42, no. 2, pp. 477–487, Apr. 2017.

[28] A. M. Lekkas and T. I. Fossen, *Line-of-Sight Guidance for Path Following of Marine Vehicles*. New York, NY, USA: Academic, 2013, ch. 5, pp. 63–91.
[29] W. Caharija, "Integral line-of-sight guidance and control of underactuated marine vehicles," Ph.D. dissertation, Dept. of Eng. Cybernetics, Norwegian Univ. Sci. Technol., Trondheim, Europe, 2014.
[30] S. Vadapalli and S. Mahapatra, "3D path following control of an autonomous underwater robotic vehicle using backstepping approach based robust state feedback optimal control law," *J. Mar. Sci. Eng.*, vol. 11, no. 2, p. 277, Jan. 2023.
[31] F. Liu, Y. Shen, B. He, J. Wan, D. Wang, Q. Yin, and P. Qin, "3DOF adaptive line-of-sight based proportional guidance law for path following of AUV in the presence of ocean currents," *Appl. Sci.*, vol. 9, no. 17, p. 3518, Aug. 2019.
[32] W. Yao and M. Cao, "Path following control in 3D using a vector field," *Automatica*, vol. 117, Jul. 2020, Art. no. 108957.
[33] S. T. Havenstrøm, A. Rasheed, and O. San, "Deep reinforcement learning controller for 3D path following and collision avoidance by autonomous underwater vehicles," *Frontiers Robot. AI*, vol. 7, pp. 1–23, Jan. 2021.
[34] G. V. Pelizer, N. B. F. da Silva, and K. R. L. J. Branco, "Comparison of 3D path-following algorithms for unmanned aerial vehicles," in *Proc. Int. Conf. Unmanned Aircr. Syst. (ICUAS)*, Jun. 2017, pp. 498–505.
[35] P. B. Sujit, S. Saripalli, and J. B. Sousa, "Unmanned aerial vehicle path following: A survey and analysis of algorithms for fixed-wing unmanned aerial vehicless," *IEEE Control Syst. Mag.*, vol. 34, no. 1, pp. 42–59, Feb. 2014.
[36] L. Degorre, "Analysis and control of autonomous underwater vehicles with reconfigurable vectoring thrust," Ph.D. dissertation, Inst. Dupuy de Lôme, Ecole Nationale d'Ingenieurs de Brest, Plouzane, France, 2023.
[37] F. Alonge, F. D'Ippolito, and F. M. Raimondi, "Trajectory tracking of underactuated underwater vehicles," in *Proc. 40th IEEE Conf. Decis. Control*, vol. 5, Jul. 2001, pp. 4421–4426.
[38] D. Yoerger and J. Slotine, "Robust trajectory control of underwater vehicles," *IEEE J. Ocean. Eng.*, vols. OE-10, no. 4, pp. 462–470, Oct. 1985.
[39] R. Cristi, F. A. Papoulias, and A. J. Healey, "Adaptive sliding mode control of autonomous underwater vehicles in the dive plane," *IEEE J. Ocean. Eng.*, vol. 15, no. 3, pp. 152–160, Jul. 1990.
[40] T. Elmokadem, M. Zribi, and K. Youcef-Toumi, "Trajectory tracking sliding mode control of underactuated AUVs," *Nonlinear Dyn.*, vol. 84, no. 2, pp. 1079–1091, Apr. 2016.
[41] M. Mat-Noh, R. Mohd-Mokhtar, M. R. Arshad, Z. M. Zain, and Q. Khan, "Review of sliding mode control application in autonomous underwater vehicles," *Indian J. Geo Mar. Sci.*, vol. 48, no. 7, pp. 973–984, 2019.
[42] T. A. Johansen and T. I. Fossen, "Control allocation—A survey," *Automatica*, vol. 49, no. 5, pp. 1087–1103, 2013.
[43] T. I. Fossen, *Handbook of Marine Craft Hydrodynamics and Motion Control*. Hoboken, NJ, USA: Wiley, 2021.
[44] H. K. Khalil, *Nonlinear Systems*, 3rd ed., Upper Saddle River, NJ, USA: Prentice-Hall, 2002.
[45] I. Barbalat, "Systmes dequations differentielles d'Oscillations non lineaires," *Rev. Math. Pures Appl.*, vol. 4, no. 2, pp. 267–270, 1959.
[46] T. I. Fossen and T. Perez. (2004). *Marine Systems Simulator (MSS)—MATLAB Toolbox*. [Online]. Available: https://github.com/cybergalactic/MSS

LOÏCK DEGORRE received the Engineering and Master of Science degrees in robotics and autonomous systems from Sorbonne Université, Paris, in 2020, and the Ph.D. degree in marine robotics and control, in 2023. He is currently a Postdoctoral Fellow with ENSTA Bretagne, Brest, France. He specializes in modeling marine robots and control systems and developing novel vector-thrust models for lightweight and agile vehicles, which are essential for underwater inspection, maintenance, and environmental observations. In Fall 2023, he further expanded his expertise as a Visiting Researcher with the Norwegian University of Science and Technology (NTNU), contributing to advanced research projects on path-following systems for autonomous underwater vehicles (AUVs). His research interests include enhancing the maneuverability and mobility of underactuated marine craft.

THOR I. FOSSEN (Fellow, IEEE) received the M.Sc. degree in marine technology, in 1987, and the Ph.D. degree in engineering cybernetics, in 1991. He is currently a Professor of guidance, navigation, and control (GNC) with the Department of Engineering Cybernetics, Norwegian University of Science and Technology. Besides cybernetics, his research fields are aerospace engineering and marine technology. This includes GNC systems for uncrewed vehicles (AUV, UAV, and USV), robotics, vehicle dynamics, and inertial navigation systems. He has been a Fulbright Scholar of flight control with the Department of Aeronautics and Astronautics, University of Washington. He is one of the co-founders and the former Vice President of research and development of Marine Cybernetics Company, which DNV acquired, in 2012. He was the Co-Founder of ScoutDI, in 2017, which develops drone-based systems for fully digitalized inspections of industrial confined spaces. He is the author of the Wiley Handbook of *Marine Craft Hydrodynamics and Motion Control* (2021). He received the Automatica Prize Paper Award and the Arch T. Colwell Merit Award from the SAE World Congress, in 2002 and 2008, respectively. He was elected to the Norwegian Academy of Technological Sciences, in 1998, and the Norwegian Academy of Science and Letters, in 2022.

EMMANUEL DELALEAU received the Diplôme d'Ingénieur degree from the Institut Supérieur d'Électronique du Nord (ISEN), in 1988, the Licence degree in pure mathematics from Lille, France, and the Ph.D. degree in control theory and the Habilitation à Diriger des Recherches degree from Paris-Saclay University, in 1993 and 2003, respectively. He was an Associate Professor with Paris-Saclay University, from 1994 to 2004. After that, he was a Professor with the Department of Mechatronics, École Nationale d'Ingénieurs de Brest, France. He is currently with the Institute Dupuy de Lôme (UMR CNRS 6027). He teaches automatic control, robotics, electrical engineering, and mathematics. His research interests include fundamental and applied control. He is involved in developing flatness-based control and model-free control, applications for underwater robotics, control of electrical motors and generators, and control of windmills and tidal turbines. He was also involved in the development of shape memory alloy actuators.

OLIVIER CHOCRON was born in Gennevilliers, France, in 1969. He received the M.Sc. degree in mechanical engineering and the Ph.D. degree in robotics from Pierre and Marie Curie University (Paris VI), in 1995 and 2000, respectively, and the Habilitation à Diriger des Recherches (H.D.R.) degree from the University of Brest (UBO), in 2023. From 2000 to 2001, he was a Postdoctoral Associate and a Lecturer with the MIT Field and Space Robotics Laboratory, Mechanical Engineering Department, Cambridge, MA, USA. From 2001 to 2002, he was a Design Engineer with European Aeronautic Defence and Space Company (EADS), on modeling, controlling, and programming military and space robotic systems. Since 2002, he has been an Associate Professor with the Department of Mechatronics, École Nationale d'Ingénieurs de Brest, Brest, France, where he teaches robotics and mechanical sciences. He joined several of the mechatronics laboratories of ENIB, CNRS, UMR, Institut de Recherche Dupuy de Lôme (IRDL), in 2016, where he researched underwater robotics. He proposed reconfigurable magnetic coupling thrusters (RMCT) technology to achieve autonomous mobility using thrust vectoring, AI-based optimization, and control. His current research interests include AUV modeling, design, and control.